Ultrasound in Medicine & Biology 000 (2025) 1–10

Contents lists available at ScienceDirect

Ultrasound in Medicine & Biology

journal homepage: www.elsevier.com/locate/ultrasmedbio

Original Contribution

High-Frequency Quantitative Ultrasound Elastography for the Mechanical Assessment of Thin Biomaterials *In Vitro*

Joseph A. Sebastian [a,b], Emmanuel Chérin [c], Eric M. Strohm [d], Zach Gouveia [b,e], Aaron Boyes [c], J. Paul Santerre [a,b,e,f], Christine E.M. Démoré [c,g], Michael C. Kolios [d,h,i], Craig A. Simmons [a,b,j,*]

[a] *Institute of Biomedical Engineering, University of Toronto, Toronto, Ontario, Canada*
[b] *Translational Biology and Engineering Program, Ted Rogers Center for Heart Research, Toronto, Ontario, Canada*
[c] *Sunnybrook Research Institute, Toronto, Ontario, Canada*
[d] *Department of Physics, Toronto Metropolitan University, Toronto, Ontario, Canada*
[e] *Faculty of Dentistry, University of Toronto, Toronto, Ontario, Canada*
[f] *Department of Chemical Engineering and Applied Chemistry, University of Toronto, Toronto, Ontario, Canada*
[g] *Department of Medical Biophysics, University of Toronto, Toronto, Ontario, Canada*
[h] *Institute of Biomedical Engineering, Science and Technology (iBEST), a partnership between Toronto Metropolitan University and St. Michael's Hospital, Toronto, Ontario, Canada*
[i] *Keenan Research Centre for Biomedical Science, Li Ka Shing Knowledge Institute, St. Michael's Hospital, Toronto, Ontario, Canada*
[j] *Department of Mechanical and Industrial Engineering, University of Toronto, Toronto, Ontario, Canada*

ARTICLE INFO

Keywords:
Biomaterials
High-frequency ultrasound
Shear modulus
shear wave elastography
acoustic attenuation

ABSTRACT

Objective: High-frequency ultrasound elastography (USE) can measure the mechanical properties of biomaterials and engineered tissues *in vitro*. Previously developed USE systems have been limited by contact acoustic radiation force (ARF) excitations and insufficient spatiotemporal resolution for sub-millimetre sub-surface mechanical property measurements.
Methods: We present a novel high-frequency USE system with a highly focused (f-number 1) 15 MHz ARF excitation transducer and a broadband (f-number 3) 40 MHz ARF tracking transducer.
Results: When comparing shear moduli measured via USE with shear rheometry, shear moduli of 1% and 5% agar-silica phantoms estimated by USE, were 8.8 ± 2.2 kPa and 117.0 ± 12.3 kPa (8.0 ± 0.4 kPa by rheometry, $p = 0.573$ for 1%; 114.4 ± 7.2 kPa, $p = 0.777$ for 5%) and oil-agar silica phantoms were 105.0 ± 3.4 kPa (0%) and 77.0 ± 22.1 kPa (10%) by USE (101.0 ± 4.8 kPa by rheometry; $p = 0.311$ for 0%; 75.8 ± 5.3 kPa; $p = 0.938$ for 10%). The speed of sound, acoustic impedance, and acoustic attenuation of these samples were also determined. We also used *in silico* analysis to mimic our experimental system and analyze the spectral content of the resulting shear waves in elastic and viscoelastic tissues with parametric changes to the ARF excitation duration, shear modulus, and viscosity. Notably, we observed a nonlinear dependency of shear wave frequency on ARF excitation duration and material properties, where shear wave frequency was most sensitive to tissue elastic modulus at longer ARF durations but more sensitive to tissue viscosity at shorter ARF durations.
Conclusion: Our system enables noninvasive, nondestructive estimation of the mechanical properties of thin biomaterials via focused axial localization of the ARF, opening new avenues for future USE applications in engineered tissue systems.

Introduction

Shear wave elastography is a widely used noninvasive and nondestructive imaging technique to probe the mechanical properties of biological tissues [1–3]. In ultrasound elastography (USE) systems (*e.g.*, shear wave elastography), the tissue is generally deformed using noninvasive methods. Noninvasive USE systems generate a remote and transient acoustic radiation force (ARF) to deform the tissue in-depth [4–7]. This deformation propagates laterally away from the axis of the ARF at a speed that increases with the tissue's shear modulus, with greater propagation speeds in stiffer tissues [1,8]. ARF-based elastography for elastographic measurements has been used to measure the mechanical properties of breast [9], Achilles tendon [10], liver [11], spleen [12], brain [13], and many other tissues [5–7,14–18].

Beyond its clinical applications, USE shows promise in measuring the mechanical properties of *in vitro* models, including engineered microtissues, organs-on-a-chip, and organoids [19–30]. Tissue elastic properties can be modulated by disease development or other factors such as the

* Corresponding author. Institute of Biomedical Engineering, University of Toronto, 661 University Avenue, 14th floor, Toronto, Ontario, M5G 1M1, Canada.
E-mail address: c.simmons@utoronto.ca (C.A. Simmons).

https://doi.org/10.1016/j.ultrasmedbio.2025.06.007
Received 12 December 2024; Revised 18 May 2025; Accepted 4 June 2025

effect of drug on the tissues in these models [31], however the latter are currently measured using *ex-situ* techniques like atomic force microscopy, nanoindentation, or tensile testing that are contact-based and incapable of monitoring elasticity over time in tissue culture [31]. Moreover, high-frequency US systems can also be integrated into conventional *in vitro* microdevice systems (*e.g.*, Transwell [32]) for deeper imaging penetration, with advantages over optical methods (*e.g.*, optical coherence elastography) that are limited by light diffraction and optical access. High-frequency (>10 MHz) USE provides noninvasive, nondestructive, and real-time monitoring capabilities, with the potential to measure tissue elastic properties with sufficient spatiotemporal resolution for thin (≤1 mm thick) microtissue models [33,34]. However, an USE system capable of measuring the mechanical properties of sub-millimetre-thick samples has yet to be developed.

There are several challenges to implementing USE for microtissue models (1) It requires highly focused high-frequency ARF transducers capable of generating transverse elastic waves in sub-millimetre thick samples and sufficient spatiotemporal resolution (*e.g.*, ~100 μm and 40 μs) to detect the propagation of elastic waves and deduce mechanical properties in both static and dynamic (*e.g.*, contracting) samples (2) Short (100−500 μs) ARF excitations are needed in both static and dynamic samples, but their short duration limits the detection of transverse waves to small distances due to the limited induced local displacements and their rapid attenuation as the wave propagates [35−45]; and (3) The complex relationship between ARF excitation duration spectral content, transverse wave attenuation, and material properties have not been studied in thin (≤ 2 mm) biomaterials. Previously published studies have aimed to overcome these challenges by using: (1) Contact and damaging shear generation techniques (*e.g.*, mechanical shaker or vibrator) that are not suitable for engineered tissues due to their lack of sterility and their tissue sample destruction potential [46−49]; or (2) Low-frequency USE systems with suboptimal spatiotemporal resolution for the assessment of sub-surface elastic wave propagation in dynamic sub-millimetre-thick samples [20−22,27,50−55].

High-frequency quantitative ultrasound elastography has shown promise as a noninvasive method for assessing the mechanical properties of biomaterials. However, its application to small, thin samples *in vitro* has been technologically limited. To overcome this challenge, we developed a high-frequency USE system with (1) tight axial localization of the ARF and increased ARF via increased ARF pulse frequency (15 MHz) and attenuation; (2) short ARF pulses (500 μs) to monitor displacements at small axial distances (mm); and in combination with these, (3) high-frequency US imaging (40 MHz) and higher imaging pulse repetition frequencies (25 kHz). Shear moduli of elastic and viscoelastic tissue phantoms measured by USE were in excellent agreement with those measured by shear rheometry. Extending our experimental work to examine shear wave spectra parametrically, *in silico* analyses revealed a nonlinear relationship between shear wave frequency, ARF excitation duration, and material properties. These findings enhance our understanding of thin biomaterials and open new avenues for future USE applications in engineered tissues and organ-on-a-chip systems.

Methods

High-frequency ultrasound system and signal acquisition

A custom-built high-frequency US system and pulsing scheme (Fig. 1) was developed to estimate the acoustic and viscoelastic properties of thin samples. This system comprises two transducers: (1) a single-element spherically focused f/3 40 MHz imaging transducer (VS40B, VisualSonics Inc, Toronto, Ontario, Canada), which was used for the estimation of attenuation, acoustic impedance, and speed of sound in the sample [24], and for shear wave tracking in elastography measurements; and (2) a custom made single-element spherically focused f/1 custom 15 MHz transducer (Device Development Lab, Sunnybrook Research Institute, Toronto, Ontario, Canada), which generated an ARF into the sample for estimation of their viscoelastic properties (Fig. 2).

The imaging transducer was excited by monocycle pulses generated by a pulse generator (Model #: AVB2-C-OCIC, Avtech Electrosystems Ltd, Nepean, ON, Canada) and transmitted through a radiofrequency (RF) switch (Mini-Circuits, Brooklyn, NY, USA). Received echoes were amplified by a 30 dB amplifier (Model # AU-2A-0150, Narda-MITEQ, Hauppauge, NY, USA) and digitized at 625 MS/s (for acoustic characterization) or 5 GS/s (for elastography measurements) by a 14-bit resolution A/D board (Teledyne SP Devices, Linköping, Sweden). For elastography measurements, the ARF transducer was excited by 15 MHz tone bursts generated by a function generator (33611A, Keysight Technologies, California, USA) and amplified by a power amplifier (A150, Electronics & Innovation, New York, USA). The duration of the ARF pulse was set to 500 μs, and its peak-peak-pressure amplitude was 9 MPa at 105 V. Both transducer pressure beams were measured using a 40-μm aperture needle hydrophone (NH0040, Precision Acoustics Ltd, Dorchester, U.K.) in a dedicated setup, and their relevant characteristics are reported in Table 1. This dual-transducer system was designed for implementation with thin (≤2 mm) engineered tissues and biomaterials. Thus, we aimed to ensure the tracking transducer was in the far field of the ARF transducer to minimize the amplitude of the ARF reflections from the surface of the tracking transducer onto the surface of our samples. In addition, we designed our ARF transducer to have a short focal zone (*i.e.*, low f-number) and tracking transducer to have a long focal zone (*i.e.*, high f-number). Lastly, to minimize sample edge effects, our transducer was designed with a -6 dB depth-of-field of 1.4 mm (*i.e.*, -3 dB depth-of-field of ~ 1 mm).

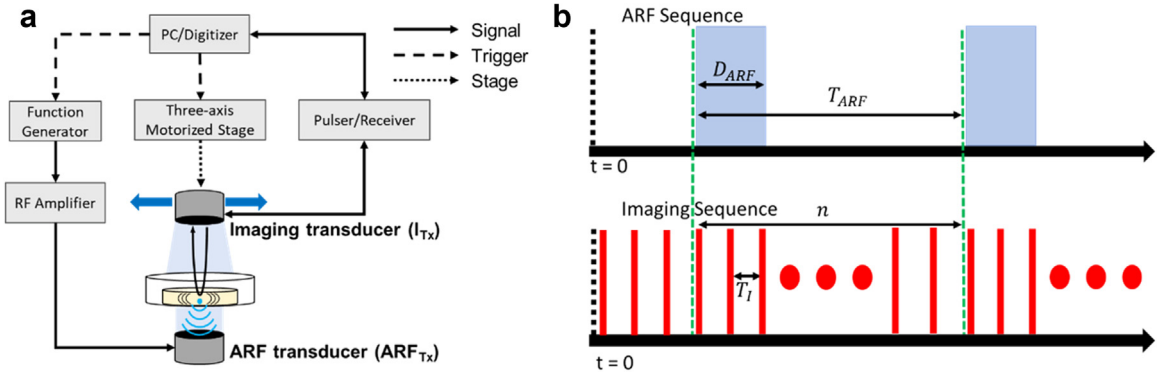

Figure 1. (a) Schematic of the experimental USE system developed for elastography measurement using a 15 MHz ARF transducer (ARF_{Tx}) and a 40 MHz imaging transducer (I_{Tx}); (b) ARF transmits (D_{ARF}: duration of ARF, $T_{ARF} = 1/PRF_{ARF}$) and imaging transmits ($T_I = 1/PRF_I$) used for RF signal acquisition. At each location, this ARF-Imaging sequence was repeated 5 times and RF lines were averaged over these iterations.

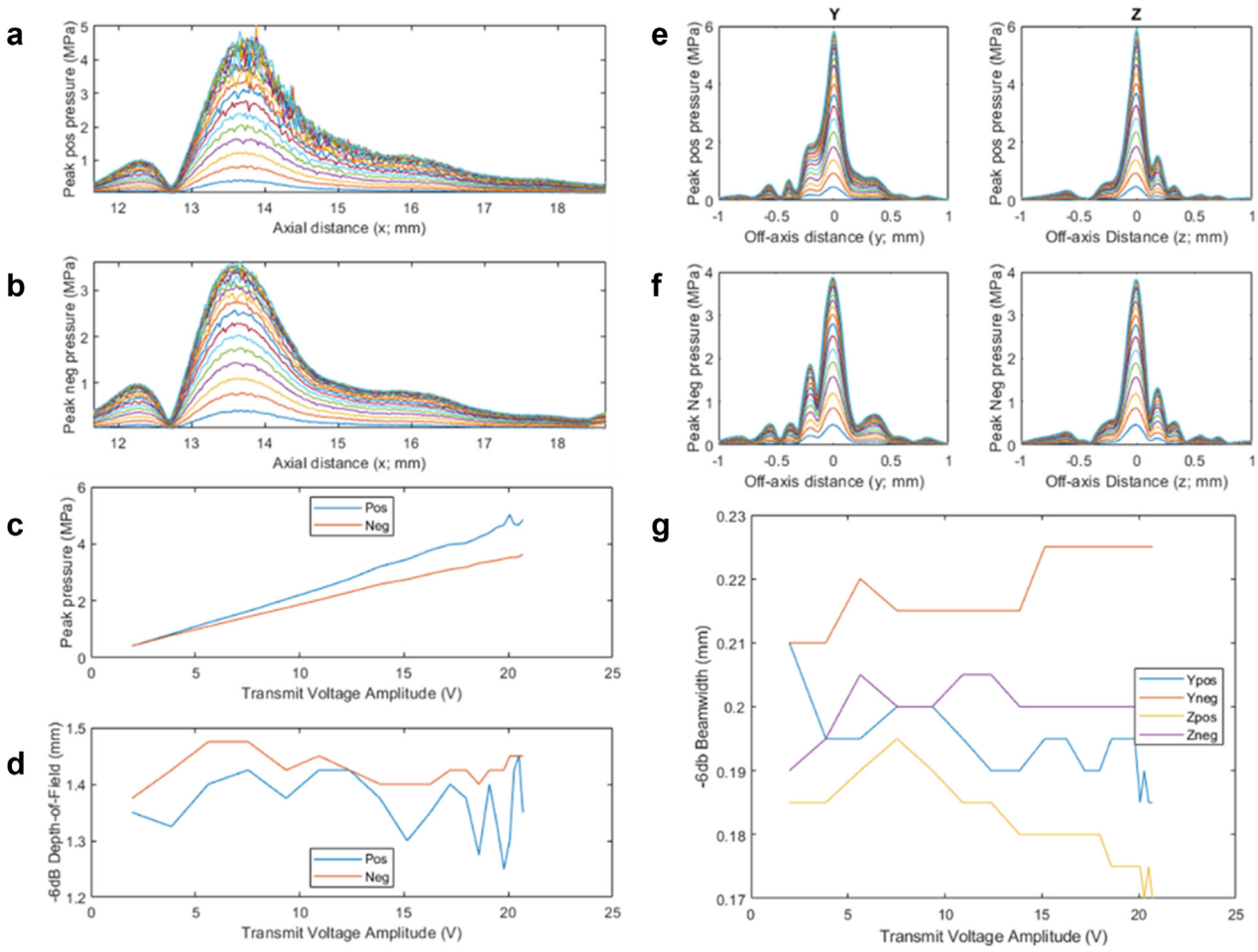

Figure 2. Hydrophone measurements of the pressure generated by the 15 MHz ARF transducer, as a function of transmit voltage amplitude. (a, b) On-axis peak (a) positive and (b) negative pressure profiles (the higher the transmit voltage amplitude, the higher the measured pressure). (c, d) Positive ('pos') and negative ('neg') pressure measured at (c) peak axial distance (~13.5–13.7 mm) and (d) -6 dB depth-of-field. (e, f) Off-axis (e) positive and (f) negative peak pressure beam profiles (at peak axial distance); (g) Variations of the -6 dB beamwidth along the Y and Z direction (at peak axial distance), for positive ('pos') and negative ('neg') peak pressures. The step size spacing of each fixed distance between each curve in (a), (b), (e), and (f) was 25 μm.

Table 1
Specifications of the two transducers in the high-frequency USE system

	ARF transducer	Imaging transducer
Center frequency (MHz)	15	40
Diameter (mm)	12.5	3
F-number	1	3
-6 dB beamwidth (μm)	200	110
Focal distance (mm)	13.6	8.56
-6 dB depth-of-field (mm)	1.4	3

Samples were positioned in a polystyrene Petri dish (Greiner Bio-One, North Carolina, USA) held by a rigid stand (MP250, Thorlabs, New Jersey, USA) and covered with water (Fig. 1a). Water was used as a coupling medium between the samples and the transducers in all experiments. The imaging transducer was affixed to a 3D-motion stage (two motorized lateral axes: Prior Scientific, USA; one manual vertical axis: MT1, Thorlabs, New Jersey, USA) and positioned above the samples. For acoustic characterization, the same acquisition procedure and processing scheme as in [24]. Briefly, the difference in the time-of-flight and ratios of the magnitudes of US signals from each interface (*e.g.*, coupling medium-substrate, sample-substrate, coupling medium-sample) were used to determine acoustic properties and RF signals were averaged 1000 times to increase SNR.

For elastography measurements, the ARF transducer was set in a fixed position below the samples, with its axis coaligned with the center of the sample. The imaging transducer was first confocally aligned with the ARF transducer, and then moved laterally away from the center axis of the ARF transducer by 100-μm increments (~ 1 beamwidth) over a scan range of ± 2.5 mm for shear wave tracking. To ensure no misalignment occurred, the transducers underwent an alignment protocol. First, the transducers were positioned facing each other and approximately focally co-aligned (using the hydrophone measurements in Fig. 2). As the tracking transducer was attached to a 3D motion stage, 3D raster scans were performed, transmitting with the push transducer and receiving with the imaging transducer to align the transducers in the X-Y direction (both transducers' centres co-aligned). Given that both transducer beams are cylindrically symmetrical, to align the transducers in the Z-direction with the pressure beam axis co-aligning with the physical axis of the transducer, we performed pulse-echo measurements with the ARF transducer, focusing the beam approximately at the front face of the other. Using the time-of-flight, the amplitude of the reflected signal, and hydrophone measurements (Fig. 2), the transducers were confocally aligned. Different scanning orientations were not explored as the samples were isotropic. The transmission and acquisition system hardware were computer-controlled using a trigger card (PB12-100-4k Pulseblaster PCI card, SpinCore Technologies, Gainesville, FL, USA) (Fig. 1b). The system was enclosed in a temperature-controlled

incubator (*In Vivo* Scientific LLC, Salem, SC, USA). For all experiments, the incubator temperature was set to 22°C.

The pulsing scheme used for shear wave tracking is represented in Figure 1b. At each location, 200 imaging pulses are transmitted at a repetition frequency PRF_I of 25 kHz and reflected signals are collected. The transmission of the 500 μs ARF pulse starts 445 μs after the transmission of the first imaging pulse so that reflected RF signals are collected before, during, and after the application of the ARF. To increase the SNR, this 8 ms sequence is repeated five times at each location and collected RF signals are averaged over these iterations. Collected RF signals were saved to a computer for offline processing and analysis using MATLAB (MathWorks, Natick, MA, USA).

Phantom fabrication and shear rheometry characterization

To produce elastic gel samples, Difco™ Technical Agar (BD Biosciences, Mississauga, ON, Canada, CAT# CA90004-032) was dissolved at 1% and 5% concentrations (w/w) in 90°C distilled water and magnetically stirred within a glass beaker on a hotplate until completely mixed (~1 hour). Agar concentration is known to modify the elastic properties of hydrogels [56]. To increase acoustic scattering and attenuation, a 2% (w/w) concentration of silicon dioxide (SiO_2) microparticles (Sigma-Aldrich, Oakville, ON, Canada, CAS# 14808-60-7) was added to the agar mixtures. Scattering is necessary to obtain detectable signals from within the samples, and attenuation is important for generating an ARF [7]. For viscoelastic samples, 10% (w/w) of castor oil (ThermoFisher Scientific, Mississauga, ON, Canada, CAT# L04224-AK) was added to 3% (w/w) agar and 2% (w/w) silicon dioxide to increase the viscosity, following the protocol in [57], such that the tan (δ) ~0.1–0.15 (via shear rheometry).

Once thoroughly mixed, the agar mixture temperature was then dropped to 40–42°C to approach its gelation point and specific volumes of the gels were pipetted into 1 mm diameter cylindrical polydimethylsiloxane (PDMS) molds within a Petri dish (Greiner Bio-One, North Carolina, USA) for acoustic measurements. For elastography measurements, 7 mm diameter holes were laser cut into the 1 mm thick bottom of Petri dishes, which was then covered on one side by a Mylar film (PolyK Technologies LLC location, SKU: PET-10.0 μm). The average thickness of the gels was 1.47 ± 0.41 mm. This provided a 7 mm diameter x 1 mm deep mold in which gels were cast. The Mylar film's acoustic properties and thickness limited the attenuation of the burst transmitted into the samples to generate the ARF. Petri dishes were then filled with distilled water at room temperature to cover the samples in their molds and placed into a 4°C fridge overnight for the samples to solidify fully.

The shear moduli of the agar-silica gels were measured using a HAAKE™ Viscotester™ iQ Rheometer (CAT# 262-0100, ThermoFisher Scientific, Massachusetts, USA) at 22°C with a 35 mm head using samples made from the same stock as those used for USE experiments. A gap height of 1 mm was used for all samples to ensure complete contact with gels. The oscillatory strain applied to all samples was between 1–5%, and the frequency sweep performed for each sample was from 0.1 to 20 Hz (higher frequencies matching shear wave frequencies could not be achieved with the rheometer). For comparison with shear moduli measured by USE, shear moduli measured by rheometry are reported as the mean storage modulus over the frequency range tested, consistent with other USE studies [20,23].

Experimental acoustic and elastic characterization

Acoustic properties (*e.g.*, speed of sound, acoustic impedance, acoustic attenuation) of thin (≤2 mm thick) agar-silica gels were measured using a previously described technique [24]. The shear modulus ($G = \rho c_s^2$) was determined via the estimated density (ρ) of the sample and the estimated shear wave velocity c_s [5,58,59], assuming an infinite, isotropic, homogenous, linear, elastic, and incompressible medium. To provide comprehensive sample characterization, we measured the acoustic properties (*e.g.*, speed of sound, acoustic attenuation, acoustic impedance, and bulk elastic modulus) in addition to the shear modulus of agar-silica and oil-agar-silica samples using high-frequency ultrasound. Acoustic properties provide critical insights into tissue mechanics and microstructure, complementing shear wave elastography. Acoustic attenuation, influenced by tissue composition and density, directly affects the generation and detection of shear waves [7] and reflects cellularity and microstructure [24]. Moreover, acoustic impedance, bulk elastic modulus, and speed of sound can quantify compressibility, elasticity, and structural variations in phantoms, cells, and tissues [60–62]. Though estimation of Young's modulus (E) is common in clinical applications of shear wave elastography via E≈3G, this analytical relationship assumes that the shear wavelength is much larger than the thickness of the samples, which does not hold in this study where the shear wavelength is on the order of the thickness of samples. Moreover, shear modulus has been used as a stiffness measure in USE studies with biomaterials [23]. To estimate the latter, the depth-dependent axial particle displacements induced by the propagating shear wave generated by ARF (Supplementary Video 1) were estimated by measuring the local temporal shifts of the imaging echoes post-ARF excitation relative to that pre-ARF excitation as a function of lateral position at the focal point of the ARF transducer (centre of the sample) as there was consistency in the waves through the depth of the biomaterial (Supplementary Fig. 1). This was done using a MATLAB cross-correlation algorithm (*xcorr*) on the reference signal that extended from -maxlag to +maxlag (window size—1000 sample points [20], window shift—500 sample points, maxlag—4500 sample points) [63] (Fig. 3a), and using *interp2* to resample and interpolate (*spline* interpolation) the data to a 4096×4096 array of lateral positions and times following methods outlined in [20]. At each lateral location, the time to displacement peak was measured at a constant depth. Finally, the shear velocity was estimated as the slope of the linear regression between lateral positions and times to displacement peak (Fig. 3b, 3c).

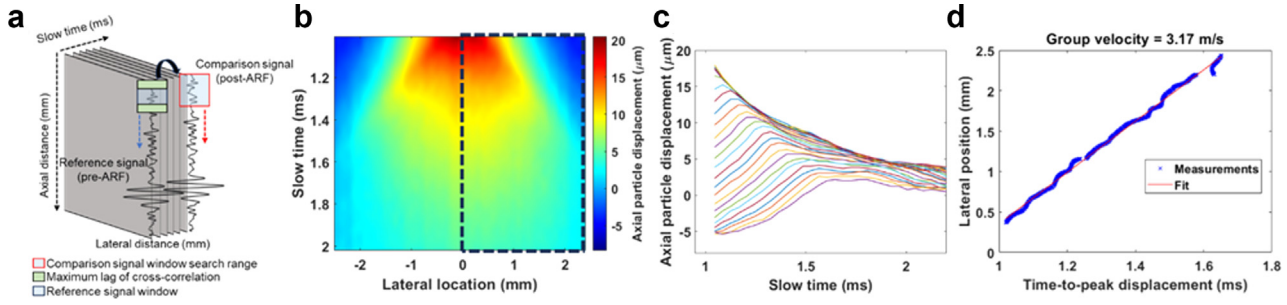

Figure 3. Signal analysis workflow. (a) Particle displacement estimation via cross-correlation. (b) Axial shear wave displacement map with black dotted line delimiting the ROI for subsequent analysis in panel c. (c) Axial particle displacement waveform over lateral position ranging from 0 to 2.5 mm for ROI indicated by black dotted line in panel b. (d) Time-to-peak vs lateral position used for group velocity estimation.

In silico *model*

While our experimental studies were aimed at measuring the elastic properties of thin biomaterials, viscous properties may also be of interest. The confocal alignment of our transducers in our USE system did not allow for viscosity measurements (see Discussion), so we computationally investigated the relationship between shear wave frequency, ARF duration, shear moduli, and viscosity in thin biomaterials, incorporating our experimental values and ARF transducer characteristics. Given the promise of USE for bioengineered tissues and materials, we examined the effects of changes in the shear moduli, viscosity, and ARF duration on the fundamental transverse wave characteristics in viscoelastic materials (*e.g.*, cell-laden hydrogels), critical for USE system development in these applications. Field II [64–66] was used to simulate the acoustic intensity field from the single-element 15 MHz ARF transducer in tissue, which was then used as input into a finite element model of an engineered microtissue that accounted for attenuative, viscoelastic and material properties of the medium (Fig. 4). The Field II simulation's properties matched our ARF transducer's (Table 1, Fig. 4a). The simulated transducer frequency was set to 15.5 MHz and a sinusoidal excitation beam. The tissue medium was simulated with an attenuation of 0.3 dB/mm, and a speed of sound of 1540 m/s was simulated to match that of the cell-laden hydrogels in our previous work [24,67]. The acoustic intensity was computed by squaring the pressure amplitude and dividing it by the density (1000 $\frac{kg}{m^3}$ [68]) and speed of sound (1540 m/s [24]).

Finite element modelling (FEM) simulations were performed using COMSOL Multiphysics 6.0 (r-6.0, Burlington, MA, USA) with an axisymmetric model geometry [69] (Fig. 4b). The simulated region was 35 mm (length) x 7 mm (height), replicating the Petri dish environment and contained a phantom (3.5 mm in radius x 1.5 mm in thickness) sandwiched between two 1.75 mm-thick coupling water layers (Fig. 4b). The focal point of the ARF's acoustic field was positioned at the centre of the tissue, as in our experimental setup (Section 2.3). Similar to [70,71], the pressure field generated by the ARF transducer was first simulated using Field II, with a transmit amplitude adjusted such that the pressure at focus was comparable to that measured experimentally with a hydrophone (Fig. 2). The duration of the transmit ARF pulse was varied from 0.1 to 0.5 ms. The output pressure field was converted from a MATLAB format (MathWorks, Natick, MA, USA) to a COMSOL-readable file using a custom MATLAB script and used to generate the body force acting on the tissue inputted in COMSOL. We used the COMSOL Solid Mechanics and Pressure module for these simulations, assuming tissue stress-strain linearity due to our configuration's observed range of local tissue deformations generated by the ARF. With regards to tissue viscoelastic properties, the bulk modulus value was set to an experimentally derived 2.32 GPa (from our previous work [24]), the shear modulus was varied in the 10–120 kPa range (from experimental observations and [23]), and the viscosity was set to 0.1 or 1 Pa•s in agreement with values reported for native heart tissue [72] and engineered tissues [23], respectively. For the elastic property simulations, the viscosity was set to 0 Pa•s. The hexagonal mesh element size was set to 17.2 μm to resolve time-dependent elastic waves spatially, and the computational time step was 10 μs. Once parametric simulations were complete, the shear wave velocity at each resolved time point and node was exported to a comma-separated-value file and analyzed in MATLAB.

Statistical analyses

Measurements were performed with at least three technical replicates for each gel condition. Statistical analyses were performed with GraphPad Prism v8.0 (San Diego, USA). All data passed the Shapiro-Wilk test for normality ($\alpha = 0.01$). The significance of the differences between the means of the acoustic properties measured in the different sample formulations and between the means of the shear moduli measured by USE and shear rheometry were investigated using unpaired Student's t-tests or Welch's t-test if variances were unequal ($\alpha = 0.01$).

Results

Acoustic and mechanical assessment of agar-silica elastic phantoms

To validate the ability of the USE system to measure the acoustic and elastic properties of thin elastic microtissues, we used ≤2 mm thick agar-silica phantoms of 1% vs. 5% agar, with a constant 2% concentration of silica dioxide microparticles (Fig. 5). There were statistically significant differences in the speed of sound ($p = 0.003$), acoustic attenuation ($p<0.0001$), and bulk elastic modulus ($p = 0.0003$) between 1% and 5% agar concentrations (Fig. 5a, 5d, 5e). The mean densities of the agar-silica phantoms (~1000 kg/m^3) were approximately that of water [68], with no significant differences between 1% and 5% agar concentrations (Fig. 5c, $p = 0.77$), similar to previous work [73]. In contrast, the acoustic attenuation coefficient measured at 40 MHz was significantly lower at 1% agar concentration vs. 5% (Fig. 5d;

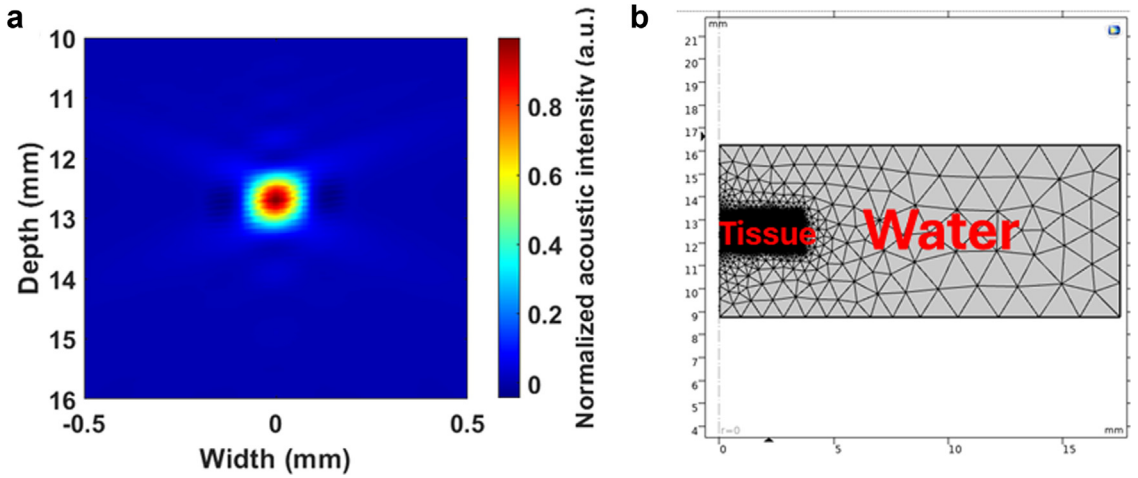

Figure 4. (a) 2D axisymmetric normalized acoustic intensity of the 15 MHz excitation transducer used in our experiments, simulated using Field II [64]. (b) Computational geometry of a 2D axisymmetric model of a 1.5 mm thick x 3.5 mm radius sample in water implemented in COMSOL Multiphysics. The radius of the Petri dish is 17.5 mm and is filled with water. The ARF transducer (not shown) is located at z = 0 mm with its center axis coaligned with the vertical axis.

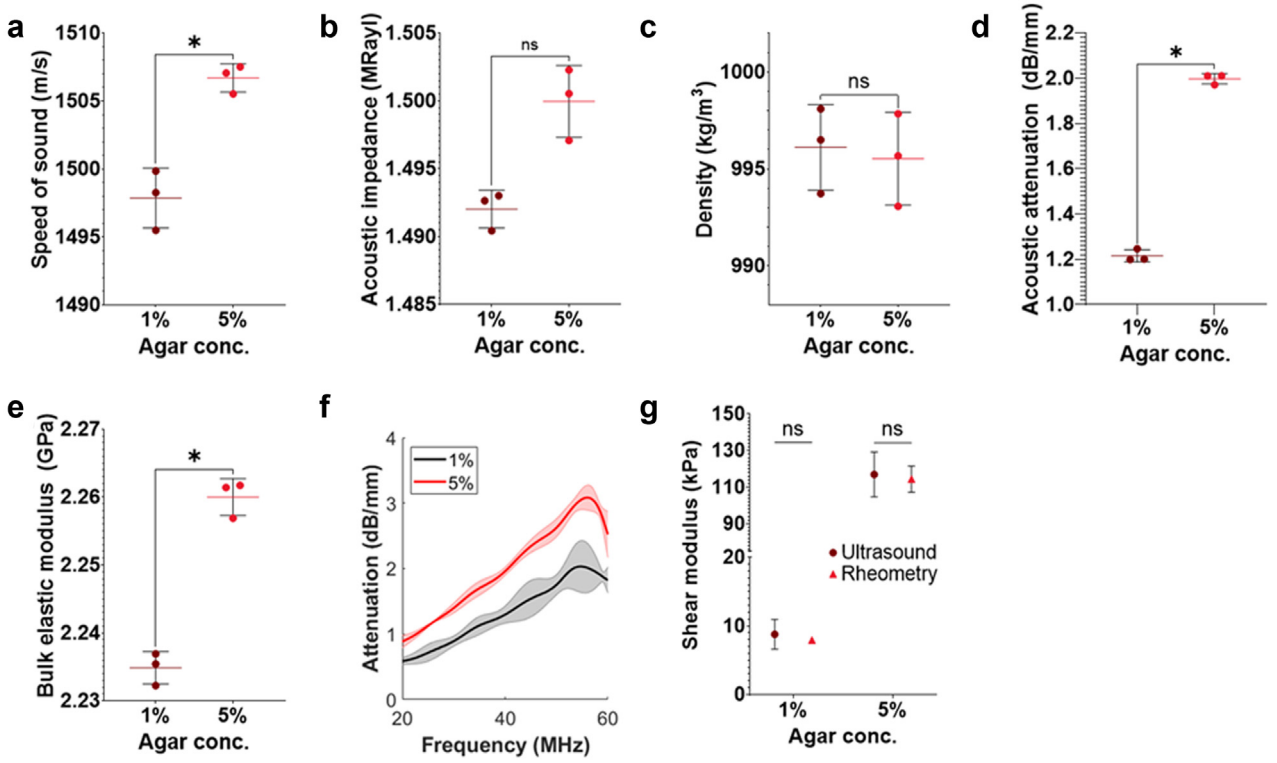

Figure 5. Acoustic and mechanical properties of agar-silica phantoms measured at two different agar concentrations: (a) speed of sound, (b) acoustic impedance, (c) density, (d) acoustic attenuation at 40 MHz, (e) bulk elastic modulus, (f) frequency-dependent attenuation within the bandwidth of the transducer (20–60 MHz), (g) shear modulus derived from the estimated shear velocity. A minimum of $n = 3$ independent phantoms was used per concentration. *Significant difference; ns, nonsignificant difference (unpaired t-test with $\alpha = 0.01$).

p<0.001). This increase was observed across the imaging transducer's bandwidth (20–60 MHz; Fig. 5f). The acoustic impedance was on the border of statistical significance (Fig. 5b; p = 0.01) due to the small sample population size.

The mean shear moduli of 1% and 5% agar-silica phantoms estimated by USE via the measurement of the group shear velocity (Section 2.2) and Eq. 1 were 8.8 ± 2.2 kPa and 117.0 ± 12.3 kPa, respectively. The USE measurements were in excellent agreement with the shear moduli measured by rheometry, with no significant differences between the two methods (8.0 ± 0.4 kPa by rheometry, p = 0.573 for 1%; 114.4 ± 7.2 kPa, p = 0.777 for 5%).

Acoustic and mechanical assessment of oil-agar-silica viscoelastic phantoms

To extend our experiments to measure the acoustic and elastic properties of thin *viscoelastic* biomaterials, we compared measurements of 3% agar-2% silica dioxide phantoms without oil (representing elastic materials, as in Section 3.1) to those with 10% castor oil, representing a viscoelastic microtissue. There were no statistically significant differences in the speed of sound (p = 0.074), acoustic impedance (p = 0.969), density (p = 0.043), and bulk elastic modulus (p = 0.174) between elastic and viscoelastic samples (Fig. 6a–c, 6e). In contrast, the acoustic attenuation coefficient measured at 40 MHz increased significantly in viscoelastic samples (Fig. 6d; p<0.001). This increase was observed across the transducer's bandwidth (20–60 MHz; Fig. 6f).

The mean shear moduli of 0% and 10% oil-agar-silica phantoms measured via USE were determined via the group velocity (Section 2.2) and Eq. 1 and compared to those measured by rheometry. There was excellent agreement between the two methods, with no significant differences (Fig. 6g): moduli measured by USE were 105.0 ± 3.4 kPa and 77.0 ± 22.1 kPa for the 0% and 10% oil phantoms, respectively, vs. 101.0 ± 4.8 kPa (p = 0.311 vs. USE) and 75.8 ± 5.3 kPa (p = 0.938) by rheometry.

Computational model validation and results

Having validated the USE system for the measurement of the elastic properties of thin biomaterials, we considered a measurement of viscous properties. Due to the confocal alignment of the transducers in our setup and the pulse sequence (*i.e.*, simultaneous imaging and radiation force excitation), our ability to detect displacement during ARF application is limited by the saturation of the imaging transducer's signal due to the ARF; as such, viscoelastic assessment via frequency-domain analysis was not possible in the current configuration. However, knowing that tighter axial focal configurations, excitation durations, and material properties (*e.g.*, viscosity) can influence the spectral content of shear waves [74], we used an *in silico* approach to examine the fundamental relationships between ARF duration and material properties in the measurement of shear wave frequency, a key factor to analytical approaches to measuring viscoelasticity using USE [75].

The *in silico* model was first validated against our experimental system and results with an isotropic, elastic 2D axisymmetric tissue model in COMSOL with dimensions replicating our experimental set up. We preset the shear modulus to 10 kPa or 120 kPa based on our experimental findings in Section 3.1 and 3.2 and determined the group velocity based on our analysis protocol in Sections 2.1 and 2.2, from which shear moduli were estimated. We found good agreement, with a percentage difference of ≤ 3% between the moduli predicted based on the COMSOL simulations (10.3 kPa and 122.3 kPa for 10 and 120 kPa shear moduli samples, respectively) and those measured experimentally (Fig. 7a–d).

We next examined the effect of changing the duration of the ARF excitation on the spectral shear wave content in thin (1.5 mm thick) linear elastic and viscoelastic tissues with a range of material properties. In both types of tissue, we observed a dominant relationship between the fundamental propagating shear wave frequency and excitation duration of $\sim 1/(2D_{ARF})$, where D_{ARF} is the duration of the ARF pulse (also alluded to in [76]) (Fig. 7e, 7f). Fundamental shear wave frequency was most

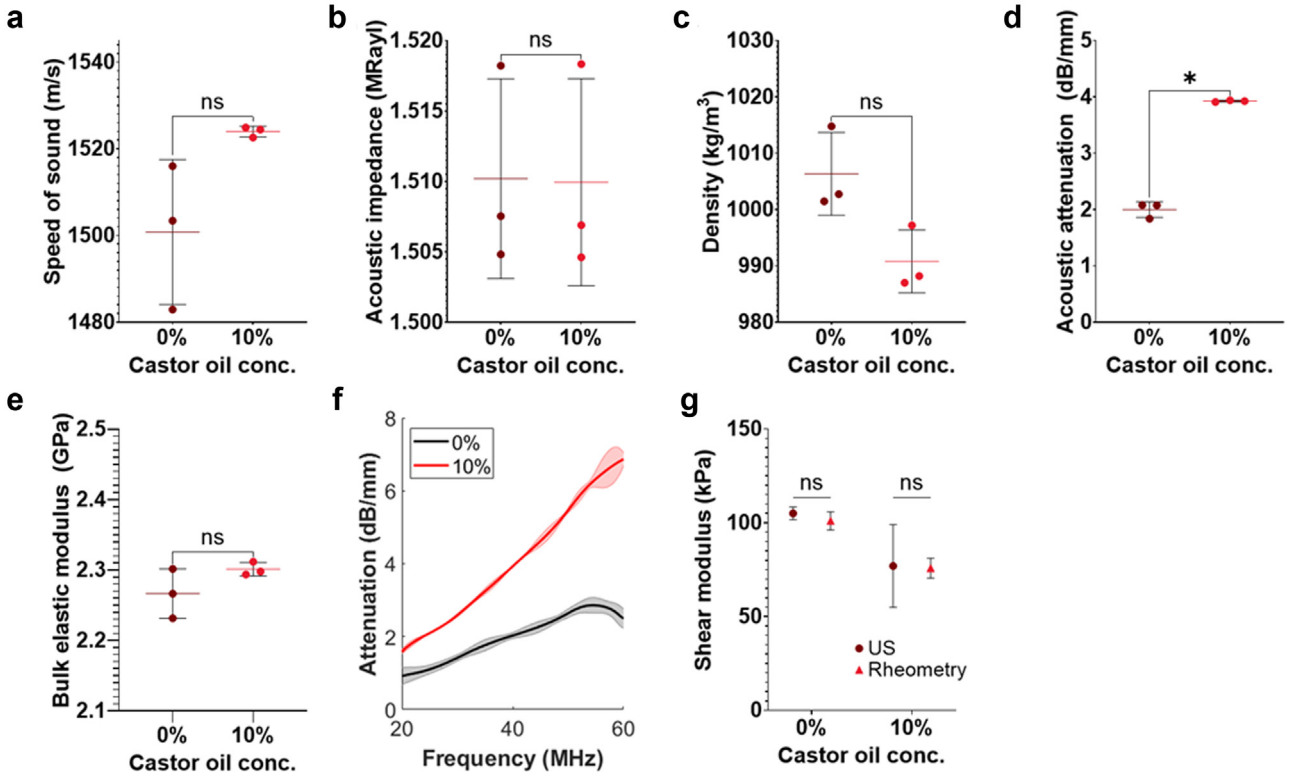

Figure 6. Measurements of the acoustic and mechanical properties of oil-agar-silica phantoms at two different oil concentrations, including (a) speed of sound, (b) acoustic impedance, (c) density, (d) acoustic attenuation at 40 MHz, (e) bulk elastic modulus, (f) frequency-dependent attenuation plot for each agar concentration within the bandwidth of the transducer (20–60 MHz), (g) shear modulus derived from the group velocity determined via shear rheometry. A minimum of $n = 3$ independent phantoms was used per concentration. *Significant difference; ns, nonsignificant difference (unpaired t-test with $\alpha = 0.01$).

sensitive to tissue elastic modulus at longer ARF durations (Fig. 7e) but more sensitive to tissue viscosity at shorter ARF durations (Fig. 7f). These results extend our experimental results beyond the capabilities of our system to understand fundamental transverse wave properties using a highly focused, high-power ARF transducer in thin biomaterials. Since shear wave attenuation increases with shear wave frequency-dependent, and shear waves attenuate faster than longitudinal waves [36], these findings inform future experimental USE systems for thin, small bioengineered tissues; in particular, longer ARF durations could yield lower frequency shear waves detectable at both longer and shorter propagation distances compared to higher frequency shear waves, and shorter ARF durations show promise to distinguish between materials of varying viscosity.

Discussion

USE is a noninvasive technique for acoustic and mechanical properties of biomaterials but has not been exploited for measurements in small, thin samples typical of *in vitro* models. Here, we developed a high-frequency USE system to estimate the acoustic and mechanical properties of thin biomaterials *in vitro*. Capitalizing on high spatiotemporal resolution, tight axial localization of the ARF, and short ARF pulses, we demonstrated accurate shear modulus measurement in elastic and viscoelastic biomaterials over a range of relevant material properties with validation by shear rheometry. Finally, we extended our experimental studies using an *in silico* approach to consider thin biomaterial viscosity and showed nonlinear dependency of fundamental shear wave frequency on ARF excitation duration and material properties, thereby informing future USE studies of thin biomaterial viscoelasticity.

The elastic agar-silica and viscoelastic oil-agar-silica phantoms used in this study were selected to model relevant tissues with a range of acoustic and material properties. The acoustic properties of the phantoms were within the ranges we measured previously for cell-seeded fibrin microtissues [24]. Of the acoustic properties measured, the speed of sound and acoustic attenuation were most sensitive to increases in agar concentration and shear moduli (Fig. 5a–f). Despite detecting a statistically significant change in the speed of sound, the relative change was negligible (<0.5%) and of minor functional significance. In contrast, the increase in acoustic attenuation (64%) with increasing agar concentration was more sizeable, likely the result of increased acoustic absorption [77]. Increased acoustic absorption is significant as it increases the ARF within the sample, potentially improving the detection of shear and guided waves via USE in our sample. In viscoelastic samples (Fig. 6a–f), the acoustic attenuation increased with oil concentration due to increased acoustic absorption with increased viscosity, which is in agreement with previous work [74]. The viscoelastic properties of the phantoms (Fig. 6g) were also within (patho)physiologically-relevant ranges. For example, the shear moduli of native heart tissue [75,76] and cardiac microtissues [77–81] range from <5 kPa for healthy tissue to >100 kPa for diseased, fibrotic tissue, and native [69] and engineered [23] cardiac tissue viscosities have been reported between 0.1 to 1 Pa•s. We measured shear moduli in the range of ~10^0 to ~10 kPa, with excellent agreement between USE and rheometry in both elastic and viscoelastic phantoms, demonstrating the robustness of the method for measurement of elastic properties of thin biomaterials of interest. Measuring these properties for USE applications in biomaterials and engineered tissues could extend to functionally assess dynamic engineered tissues and organ-on-a-chip systems.

Measurement of viscous properties via USE requires frequency domain analysis of shear wave signals [38,78–80]. We could not do these measurements with our current setup because the confocal alignment of the transducers and pulse sequence (*i.e.*, simultaneous imaging and radiation force excitation) reduces the ARF due to multiple reflections by the two transducers. Moreover, this setup inhibits our imaging

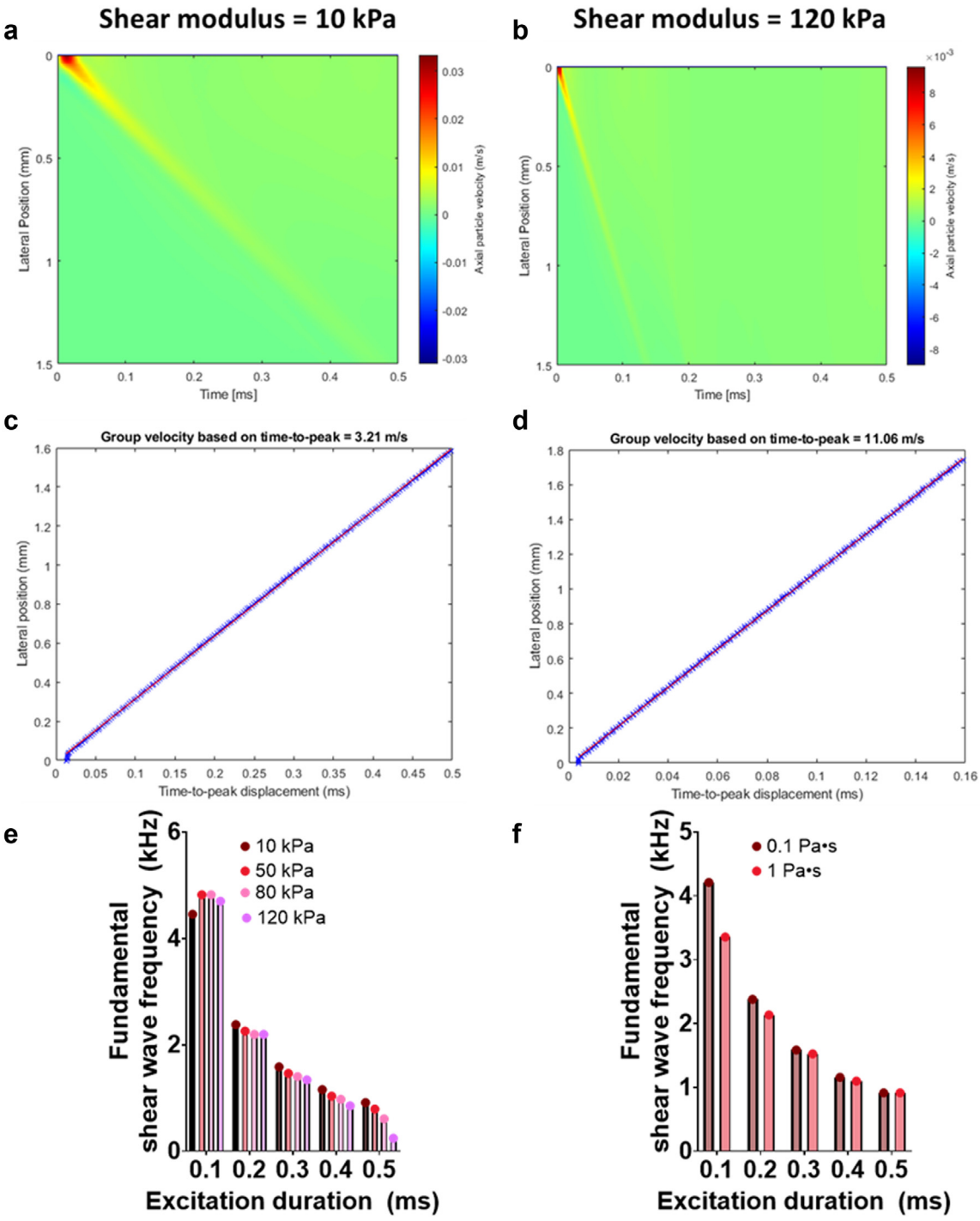

Figure 7. Simulation of a shear wave propagating in a linear, isotropic, purely elastic (shear viscosity = 0 Pa•s) sample with shear modulus of (a) 10 kPa and (b) 120 kPa. The shear wave velocity is estimated as the slope of the lateral position vs. time-to-peak curve in (c) and (d). The estimated shear moduli are within 3% of the preset shear moduli. Shear wave peak frequency measured at a lateral distance of 2 mm and as a function of ARF pulse duration in (e) four linear, isotropic, elastic materials of various elastic moduli and in (f) two viscoelastic materials of different viscosity with a fixed shear modulus of 10 kPa.

transducer's ability to detect displacement during ARF application due to the saturation of the imaging transducer's signal due to ARF. Thus, our analysis protocol (Section 2.2) proceeds after the ARF application is completed and until the shear wave attenuates to a zero-amplitude signal or the lateral edge of the static sample. This results in a significant zero-frequency component in our spectral axial displacement data, inhibiting our ability to do spectral analysis and viscoelasticity measurements via ultrasound, and directly comparing frequency-dependent shear modulus curves in the relevant frequency range. Although multiple wave types propagate in these samples (*e.g.*, Lamb), detected via spectral analysis, we used group velocity to estimate the shear moduli of both elastic and viscoelastic media, as shear waves dominate the axial particle displacement compared to other wave propagations [59,81]. The excellent agreement we observed between USE and rheometry shear moduli measurements (Figs. 5G, 6G) validates this approach. To enable viscosity measurements, a custom narrow band-stop filter could be used

to remove ARF pulse fundamental and harmonic components from the ARF transducer, or a dual-frequency transducer could be used. Moreover, for more precise and convergent measurements of the -6 dB beamwidth, more input transmit voltages could be used. Future work will focus on the development of a USE system that overcomes these limitations via a bandpass filter or dual-frequency transducer, enabling the use of phase velocity to evaluate stiffness, as it may yield more accurate shear and Young's modulus estimates [82].

Conclusion

We report a noninvasive and nondestructive high-frequency quantitative ultrasound elastography system to estimate the mechanical properties of thin biomaterials *in vitro* with high spatiotemporal resolution (~100 μm, 5 GHz sampling, 25 kHz pulse repetition frequency). Shear moduli of elastic and viscoelastic tissue phantoms measured by USE were in excellent agreement with those measured by shear rheometry. *In silico* analyses revealed the nonlinear dependency of fundamental shear wave frequency on ARF excitation duration and material properties, informing future USE studies aimed at measuring the viscoelastic properties of thin biomaterials. Promising future applications based on the high spatiotemporal resolution of this technique could extend to dynamic engineered tissues and organ-on-a-chip systems.

Data availability

The data that support the findings of this study are available from the corresponding author upon reasonable request.

Conflict of interest

All authors declare no competing interests.

Acknowledgments

This work was supported by a Collaborative Health Research Program grant from the Natural Science and Engineering Research Council of Canada (NSERC; CHRPJ 5083) and the Canadian Institutes of Health Research (CPG-151946). J.A.S. was supported by an NSERC Canada Graduate Scholarship—Master's, a University of Toronto-National Research Council Centre for Research and Applications in Fluidic Technologies (CRAFT) Doctoral Fellowship, an NSERC Collaborative Research and Training Experience (CREATE) Doctoral Fellowship, a Connaught PhD for Public Impact Fellowship, and an NSERC Vanier Canada Graduate Scholarship.

Supplementary materials

Supplementary material associated with this article can be found in the online version at doi:10.1016/j.ultrasmedbio.2025.06.007.

References

[1] Li GY, Cao Y. Mechanics of ultrasound elastography. Proc R Soc A 2017;473 (2199):20160841.
[2] Nenadic IZ, editor. Handbook of ultrasound elastography: biomedical applications and medicine. Hoboken, NJ: Wiley; 2018.
[3] Chen X, Li X, Turco S, Van Sloun RJG, Mischi M. Ultrasound viscoelastography by acoustic radiation force: a state-of-the-art review. IEEE Trans Ultrason Ferroelect Freq Contr 2024.
[4] Parker KJ, Taylor LS, Gracewski S, Rubens DJ. A unified view of imaging the elastic properties of tissue. J Acoust Soc Am 2005;117(5):2705–12.
[5] Sarvazyan AP, Rudenko OV, Swanson SD, Fowlkes JB, Emelianov SY. Shear wave elasticity imaging: a new ultrasonic technology of medical diagnostics. Ultrasound Med Biol 1998;24(9):1419–35.
[6] Sarvazyan AP, Rudenko OV, Nyborg WL. Biomedical applications of radiation force of ultrasound: historical roots and physical basis. Ultrasound Med Biol 2010;36 (9):1379–94.
[7] Sarvazyan AP, Rudenko OV, Fatemi M. Acoustic radiation force: a review of four mechanisms for biomedical applications. IEEE Trans Ultrason Ferroelect Freq Contr 2021;68(11):3261–9.
[8] Palmeri ML, Sharma AC, Bouchard RR, Nightingale RW, Nightingale KR. A finite-element method model of soft tissue response to impulsive acoustic radiation force. IEEE Trans Ultrason Ferroelect Freq Contr 2005;52(10):1699–712.
[9] Bercoff J, Chaffai S, Tanter M, Sandrin L, Catheline S, Fink M, et al. In vivo breast tumor detection using transient elastography. Ultrasound Med Biol 2003;29(10):1387–96.
[10] Brum J, Bernal M, Gennisson JL, Tanter M. *In vivo* evaluation of the elastic anisotropy of the human Achilles tendon using shear wave dispersion analysis. Phys Med Biol 2014;59(3):505–23.
[11] Kim JR, Suh CH, Yoon HM, Lee JS, Cho YA, Jung AY. The diagnostic performance of shear-wave elastography for liver fibrosis in children and adolescents: A systematic review and diagnostic meta-analysis. Eur Radiol 2018;28(3):1175–86.
[12] Hassan K, Loberant N, Abbas N, Fadi H, Shadia H, Khazim K. Shear wave elastography imaging for assessing the chronic pathologic changes in advanced diabetic kidney disease. TCRM 2016;12:1615–22.
[13] Imbault M, Demene C, Mossad M, Jl Gennisson, Tanter M, Chauvet D, et al. Intraoperative quantitative measurement of brain tumor stiffness and intracranial pressure assessment using ultrasound shear wave elastography. 2014 IEEE International Ultrasonics Symposium. Chicago, IL, USA: IEEE; 2014. p. 201–4http://ieeexplore.ieee.org/document/6932200/.
[14] Barbone PE, Oberai AA, Hall TJ. Introduction to quasi-static elastography. Tissue Elasticity Imaging. Elsevier; 2020. p. .61–83https://linkinghub.elsevier.com/retrieve/pii/B9780128096611000042.
[15] Lerner RM, Huang SR, Parker KJ. "Sonoelasticity" images derived from ultrasound signals in mechanically vibrated tissues. Ultrasound Med Biol 1990;16(3):231–9.
[16] Chen S, Fatemi M, Greenleaf JF. Remote measurement of material properties from radiation force induced vibration of an embedded sphere. J Acoust Soc Am 2002;112(3):884–9.
[17] Fatemi M, Greenleaf JF. Ultrasound-Stimulated Vibro-Acoustic Spectrography. Science 1998;280(5360):82–5.
[18] Dutt V, Kinnick RR, Greenleaf JF. Acoustic shear wave displacement measurement using ultrasound. 1996 IEEE Ultrasonics Symposium Proceedings. San Antonio, TX, USA: IEEE; 1996. p. 1185–8http://ieeexplore.ieee.org/document/584202/.
[19] Chao PY, Liu WW, You SF, Li PC. Shear wave elasticity measurements of three-dimensional cancer cell cultures using laser speckle contrast imaging. Sci Rep 2018;8 (1):14470.
[20] Kuo PL, Charng CC, Wu PC, Li PC. Shear-wave elasticity measurements of three-dimensional cell cultures for mechanobiology. J Cell Sci 2017;130(1):292–302.
[21] Hong X, Stegemann JP, Deng CX. Microscale characterization of the viscoelastic properties of hydrogel biomaterials using dual-mode ultrasound elastography. Biomaterials 2016;88:12–24.
[22] Hong X, Annamalai RT, Kemerer TS, Deng CX, Stegemann JP. Multimode ultrasound viscoelastography for three-dimensional interrogation of microscale mechanical properties in heterogeneous biomaterials. Biomaterials 2018;178:11–22.
[23] Hobson EC, Li W, Juliar BA, Putnam AJ, Stegemann JP, Deng CX. Resonant acoustic rheometry for non-contact characterization of viscoelastic biomaterials. Biomaterials 2021;269:120676.
[24] Sebastian JA, Strohm EM, Chérin E, Mirani B, Démoré C, Kolios MC, et al. High-frequency quantitative ultrasound for the assessment of the acoustic properties of engineered tissues in vitro. Acta Biomater 2022:S1742706122008170.
[25] Strohm EM, Callaghan NI, Ding Y, Latifi N, Rafatian N, Funakoshi S, et al. Noninvasive quantification of contractile dynamics in cardiac cells, spheroids, and organs-on-a-chip using high-frequency ultrasound. ACS Nano 2024;18(1):314–27.
[26] Hobson EC, Li W, Friend NE, Putnam AJ, Stegemann JP, Deng CX. Crossover of surface waves and capillary-viscous-elastic transition in soft biomaterials detected by resonant acoustic rheometry. Biomaterials 2023;302:122282.
[27] Lu SL, Chao PY, Liu WW, Han K, Cheng JCH, Li PC. Longitudinal shear wave elasticity measurements of millimeter-sized biomaterials using a single-element transducer platform. Cloutier G, editor. PLoS ONE 2022;17(4):e0266235.
[28] Shih CC, Qian X, Ma T, Han Z, Huang CC, Zhou Q, et al. Quantitative assessment of thin-layer tissue viscoelastic properties using ultrasonic micro-elastography with lamb wave model. IEEE Trans Med Imaging 2018;37(8):1887–98.
[29] Mercado KP, Langdon J, Helguera M, McAleavey SA, Hocking DC, Dalecki D. Scholte wave generation during single tracking location shear wave elasticity imaging of engineered tissues. J Acoust Soc Am 2015;138(2):EL138–44.
[30] Ingber DE. Is it time for reviewer 3 to request human organ chip experiments instead of animal validation studies? Adv Sci 2020;7(22):2002030.
[31] Guimarães CF, Gasperini L, Marques AP, Reis RL. The stiffness of living tissues and its implications for tissue engineering. Nat Rev Mater 2020;5(5):351–70.
[32] Strohm EM, Callaghan NI, Ding Y, Latifi N, Rafatian N, Funakoshi S, et al. Noninvasive quantification of contractile dynamics in cardiac cells, spheroids, and organs-on-a-chip using high-frequency ultrasound. ACS Nano 2024;18(1):314–27.
[33] Park SE, Georgescu A, Huh D. Organoids-on-a-chip. Science 2019;364(6444):960–5.
[34] Zhao Y, Rafatian N, Feric NT, Cox BJ, Aschar-Sobbi R, Wang EY, et al. A platform for generation of chamber-specific cardiac tissues and disease modeling. Cell 2019;176 (4):913–927.e18.
[35] Philip J, Basu BK, Samudravijaya K. Ultrasonic attenuation of longitudinal and shear waves in superconducting lead. J Low Temp Phys 1987;67(5–6):453–74.
[36] Wu J. Determination of velocity and attenuation of shear waves using ultrasonic spectroscopy. J Acoust Soc Am 1996;99(5):2871–5.
[37] Zhao H, Urban M, Greenleaf J, Chen S. Elasticity and viscosity estimation from shear wave velocity and attenuation: A simulation study. 2010 IEEE International Ultrasonics Symposium. San Diego, CA, USA: IEEE; 2010. p. 1604–7http://ieeexplore.ieee.org/document/5935462/.

[38] Nenadic IZ, Urban MW, Bernal M, Greenleaf JF. Phase velocities and attenuations of shear, Lamb, and Rayleigh waves in plate-like tissues submerged in a fluid (L). J Acoust Soc Am 2011;130(6):3549–52.
[39] Amador Carrascal C, Aristizabal S, Greenleaf JF, Urban MW. Phase aberration and attenuation effects on acoustic radiation force-based shear wave generation. IEEE Trans Ultrason Ferroelect Freq Contr 2016;63(2):222–32.
[40] Bernard S, Kazemirad S, Cloutier G. A frequency-shift method to measure shear-wave attenuation in soft tissues. IEEE Trans Ultrason Ferroelectr Freq Control 2017;64 (3):514–24.
[41] Nenadic IZ, Qiang B, Urban MW, Zhao H, Sanchez W, Greenleaf JF, et al. Attenuation measuring ultrasound shearwave elastography and in vivo application in post-transplant liver patients. Phys Med Biol 2017;62(2):484–500.
[42] Lipman SL, Rouze NC, Palmeri ML, Nightingale KR. Impact of acoustic radiation force excitation geometry on shear wave dispersion and attenuation estimates. Ultrasound Med Biol 2018;44(4):897–908.
[43] Chintada BR, Rau R, Goksel O. Nonlinear Characterization of Tissue Viscoelasticity with Acoustoelastic Attenuation of Shear-Waves. . 2020 [accessed 21.04.20]; Available from: http://arxiv.org/abs/2002.12908
[44] Kijanka P, Urban MW. Two-point frequency shift method for shear wave attenuation measurement. IEEE Trans Ultrason Ferroelectr Freq Control 2020;67(3):483–96.
[45] Kijanka P, Urban MW. Improved two-point frequency shift power method for measurement of shear wave attenuation. Ultrasonics 2022;124:106735.
[46] Lee S, Eun LY, Hwang JY, Eun Y. Ex vivo evaluation of mechanical anisotropic tissues with high-frequency ultrasound shear wave elastography. Sensors 2022;22(3):978.
[47] Qian X, Li R, Lu G, Jiang L, Kang H, Kirk Shung K, et al. Ultrasonic elastography to assess biomechanical properties of the optic nerve head and peripapillary sclera of the eye. Ultrasonics 2021;110:106263.
[48] Qian X, Ma T, Shih CC, Heur M, Zhang J, Shung KK, et al. Ultrasonic microelastography to assess biomechanical properties of the cornea. IEEE Trans Biomed Eng 2019;66(3):647–55.
[49] Lay FY, Chen PY, Cheng HF, Kuo YM, Huang CC. *Ex vivo* evaluation of mouse brain elasticity using high-frequency ultrasound elastography. IEEE Trans Biomed Eng 2019;66(12):3426–35.
[50] Jeng GS, Yeh CL, Lee CL, Yang YS, Tseng LY, Li PC. Ultrasound shear-wave computed tomography for elasticity imaging. Appl Phys Lett 2022;121(4):043702.
[51] Qian X, Ma T, Yu M, Chen X, Shung KK, Zhou Q. Multi-functional ultrasonic micro-elastography imaging system. Sci Rep 2017;7(1):1230.
[52] Shih CC, Qian X, Ma T, Han Z, Huang CC, Zhou Q, et al. Quantitative assessment of thin-layer tissue viscoelastic properties using ultrasonic micro-elastography with lamb wave model. IEEE Trans Med Imaging 2018;37(8):1887–98.
[53] Lu G, Li R, Qian X, Chen R, Jiang L, Chen Z, et al. Layer-specific ultrasound elastography using a multi-layered shear wave dispersion model for assessing the viscoelastic properties. Phys Med Biol 2020 [accessed 18.11.20]; Available from: https://iopscience.iop.org/article/10.1088/1361-6560/abca04.
[54] Kim S, Moon S, Rho S, Yoon S. Measurements of acoustic radiation force of ultrahigh frequency ultrasonic transducers using model-based approach. Appl Phys Lett 2021;118(18):184102.
[55] Mercado KP, Helguera M, Hocking DC, Dalecki D. Noninvasive quantitative imaging of collagen microstructure in three-dimensional hydrogels using high-frequency ultrasound. Tissue Eng C: Methods 2015;21(7):671–82.
[56] Manickam K, Machireddy RR, Seshadri S. Characterization of biomechanical properties of agar based tissue mimicking phantoms for ultrasound stiffness imaging techniques. J Mech Behav Biomed Mater 2014;35:132–43.
[57] Nguyen MM, Zhou S, luc Robert J, Shamdasani V, Xie H. Development of oil-in-gelatin phantoms for viscoelasticity measurement in ultrasound shear wave elastography. Ultrasound Med Biol 2014;40(1):168–76.
[58] Alam SK, Garra B, editors. Tissue elasticity imaging: volume 1: theory and methods. 1st ed. San Diego: Elsevier Inc; 2020.
[59] Rouze NC, Deng Y, Trutna CA, Palmeri ML, Nightingale KR. Characterization of viscoelastic materials using group shear wave speeds. IEEE Trans Ultrason Ferroelectr Freq Control 2018;65(5):780–94.
[60] Cafarelli A, Verbeni A, Poliziani A, Dario P, Menciassi A, Ricotti L. Tuning acoustic and mechanical properties of materials for ultrasound phantoms and smart substrates for cell cultures. Acta Biomater 2017;49:368–78.
[61] Strohm EM, Czarnota GJ, Kolios MC. Quantitative measurements of apoptotic cell properties using acoustic microscopy. IEEE Trans Ultrason Ferroelect Freq Contr 2010;57(10):2293–304.
[62] Saijo Y, Tanaka M, Okawai H, Sasaki H, Nitta SI, Dunn F. Ultrasonic tissue characterization of infarcted myocardium by scanning acoustic microscopy. Ultrasound Med Biol 1997;23(1):77–85.
[63] Luo Jianwen, Konofagou EE. A fast normalized cross-correlation calculation method for motion estimation. IEEE Trans Ultrason Ferroelect Freq Contr 2010;57(6):1347–57.
[64] Jensen JA, Svendsen NB. Calculation of pressure fields from arbitrarily shaped, apodized, and excited ultrasound transducers. IEEE Trans Ultrason Ferroelect Freq Contr 1992;39(2):262–7.
[65] Jensen JA. A model for the propagation and scattering of ultrasound in tissue. J Acoust Soc Am 1991;89(1):182–90.
[66] Jensen JA. Simulation of advanced ultrasound systems using Field II. 2004 2nd IEEE International Symposium on Biomedical Imaging: Macro to Nano (IEEE Cat No 04EX821). Arlington, VA, USA: IEEE; 2004. p. 636–9http://ieeexplore.ieee.org/document/1398618/.
[67] Pinkerton JMM. The absorption of ultrasonic waves in liquids and its relation to molecular constitution. Proc Phys Soc B 1949;62(2):129–41.
[68] Madsen EL, Deaner ME, Mehi J. Properties of phantom tissuelike polymethylpentene in the frequency range 20−70 MHZ. Ultrasound Med Biol 2011;37 (8):1327–39.
[69] Palmeri ML, Qiang B, Chen S, Urban MW. Guidelines for finite-element modeling of acoustic radiation force-induced shear wave propagation in tissue-mimicking media. IEEE Trans Ultrason Ferroelect Freq Contr 2017;64(1):78–92.
[70] Goswami S, Ahmed R, Khan S, Doyley MM, McAleavey SA. Shear induced non-linear elasticity imaging: elastography for compound deformations. IEEE Trans Med Imaging 2020;39(11):3559–70.
[71] Goswami S, Ahmed R, Feng F, Khan S, Doyley MM, McAleavey SA. Imaging the local nonlinear viscoelastic properties of soft tissues: initial validation and expected benefits. IEEE Trans Ultrason Ferroelect Freq Contr 2022;69(3):975–87.
[72] Urban MW, Pislaru C, Nenadic IZ, Kinnick RR, Greenleaf JF. Measurement of viscoelastic properties of in vivo swine myocardium using lamb wave dispersion ultrasound vibrometry (LDUV). IEEE Trans Med Imaging 2013;32(2):247–61.
[73] Chen P, Pollet AMAO, Panfilova A, Zhou M, Turco S, Den Toonder JMJ, et al. Acoustic characterization of tissue-mimicking materials for ultrasound perfusion imaging research. Ultrasound Med Biol 2022;48(1):124–42.
[74] Palmeri ML, Deng Yufeng, Rouze NC, Nightingale KR. Dependence of shear wave spectral content on acoustic radiation force excitation duration and spatial beamwidth. 2014 IEEE International Ultrasonics Symposium. Chicago, IL, USA: IEEE; 2014. p. 1105–8http://ieeexplore.ieee.org/document/6931899/.
[75] Li H, Flé G, Bhatt M, Qu Z, Ghazavi S, Yazdani L, et al. Viscoelasticity imaging of biological tissues and single cells using shear wave propagation. Front Phys 2021;9:666192.
[76] Zvietcovich F, Larin KV. Wave-based optical coherence elastography: the 10-year perspective. Prog Biomed Eng 2022;4(1):012007.
[77] Sebastian JA, Strohm EM, Baranger J, Villemain O, Kolios MC, Simmons CA. Assessing engineered tissues and biomaterials using ultrasound imaging: In vitro and in vivo applications. Biomaterials 2023;296:122054.
[78] Kijanka P, Urban MW. Local phase velocity based imaging: a new technique used for ultrasound shear wave elastography. IEEE Trans Med Imaging 2019;38(4):894–908.
[79] Parker KJ, Ormachea J, Hah Z. Group versus phase velocity of shear waves in soft tissues. Ultrason Imaging 2018;40(6):343–56.
[80] Kijanka P, Urban MW. Phase velocity estimation with expanded bandwidth in viscoelastic phantoms and tissues. IEEE Trans Med Imaging 2021;40(5):1352–62.
[81] Trutna CA, Rouze NC, Palmeri ML, Nightingale KR. Measurement of viscoelastic material model parameters using fractional derivative group shear wave speeds in simulation and phantom data. IEEE Trans Ultrason Ferroelect Freq Contr 2020;67 (2):286–95.
[82] Maksuti E, Widman E, Larsson D, Urban MW, Larsson M, Bjällmark A. Arterial stiffness estimation by shear wave elastography: validation in phantoms with mechanical testing. Ultrasound Med Biol 2016;42(1):308–21.